

# QCD thermodynamics with continuum extrapolated dynamical overlap fermions

Sz. Borsanyi<sup>a</sup>, Z. Fodor<sup>a,b,c</sup>, S.D. Katz<sup>c,d</sup>, S. Krieg<sup>a,b</sup>, T. Lippert<sup>a,b</sup>, D. Nogradi<sup>c,d</sup>, F. Pittler<sup>c,d</sup>,  
K.K. Szabo<sup>a,b</sup>, B.C. Toth<sup>a</sup>

<sup>a</sup>*Department of Physics, Wuppertal University, Gausstrasse 20, D-42119 Wuppertal, Germany*

<sup>b</sup>*IAS/JSC, Forschungszentrum Jülich, D-52425 Jülich, Germany*

<sup>c</sup>*Institute for Theoretical Physics, Eötvös University, Pázmány Peter sétány 1/A, H-1117 Budapest, Hungary*

<sup>d</sup>*MTA-ELTE Lendület Lattice Gauge Theory Research Group, Budapest, Hungary*

---

## Abstract

We study the finite temperature transition in QCD with two flavors of dynamical fermions at a pseudoscalar pion mass of about 350 MeV. We use lattices with temporal extent of  $N_t=8, 10$  and  $12$ . For the first time in the literature a continuum limit is carried out for several observables with dynamical overlap fermions. These findings are compared with results obtained within the staggered fermion formalism at the same pion masses and extrapolated to the continuum limit. The presented results correspond to fixed topology and its effect is studied in the staggered case. Nice agreement is found between the overlap and staggered results.

*Keywords:* Lattice QCD, Chiral fermions, Finite temperature QCD

---

## 1. Introduction

The QCD Lagrangian possesses an approximate  $SU(2)_V \times SU(2)_A \times U(1)_V \times U(1)_A$  global symmetry. Both  $SU(2)$  symmetries and  $U(1)_A$  are explicitly broken by small mass effects.  $SU(2)_A$  is spontaneously broken even in the massless limit and the  $U(1)_A$  is always broken on the quantum level by the chiral anomaly. According to the most popular picture the QCD transition at non-vanishing temperatures is related to the restoration of the  $SU(2)_A$  chiral symmetry. Though for physical quark masses the transition turns out to be an analytic cross-over [1] the physics of the transition is still determined by the remnants of the above mentioned symmetry breaking and its restoration.

The staggered fermion formulation is the cheapest one among all lattice fermion formulations used for QCD. In addition, staggered fermions possess a chiral symmetry even at non-vanishing lattice spacings. Thus, they show the most important physical feature of the finite temperature QCD transition already at non-zero lattice spacings. These two features, low CPU demand and symmetry, explain why almost all large-scale lattice thermodynamics projects use staggered fermions. For many bulk quantities reliable quantitative results exist. These are obtained by controlled continuum extrapolations. E.g. the scale of the temperature was calculated [2, 3, 4, 5] in physical units and the equation of state was determined [6, 7, 8].

Though staggered fermions possess a chiral symmetry, it is not the same as that of the continuum QCD theory. In addition, there is a subtle procedure how this chiral symmetry is broken, how it is restored and how to look at it for less than four flavors by rooting. Besides the theoretical difficulties related to staggered fermions, there are technical difficulties, too. First of all, the observables, that are related to pion physics suffer from large discretization effects related to the taste symmetry violation (see e.g. [9] for examples). Secondly, measuring the thermal correlations of quarks and hadrons is notoriously difficult, due to the complicated valence structure of staggered quarks.

Wilson fermions do not possess any chiral symmetry at non-vanishing lattice spacings, the symmetry is restored only in the continuum limit. As a consequence Wilson fermion based thermodynamics has large cutoff effects and small lattice spacings are needed to carry out controlled continuum extrapolations [10, 11].

Chiral lattice fermions (overlap or domain-wall) are ideal candidates for lattice QCD thermodynamics. Obviously, they are much more expensive than the staggered discretization. Since the first dynamical overlap study [12] there have been a number of finite temperature results using overlap [13, 14] or domain wall [15, 16, 17] fermions. These works used  $N_t = 6$  and/or  $N_t = 8$  lattice extents. Until now, no larger temporal extents were used and no continuum extrapolation was performed. The main goal of this paper is to present the very first investigation of this kind.

In this paper we continue our thermodynamic investigations with overlap fermions started in 2012 in Ref. [14]. We had two lattice spacings back then,  $N_t=6$  and 8. Here we go far beyond that level and extend that work with two finer sets of lattice spacings,  $N_t=10$  and 12. Since the action, the observables and many of the methods are the same as in our first paper, here we only describe them briefly and focus on the novel features and improvements. Then we present results with three temporal extents:  $N_t=8,10$  and 12 for four observables. We carry out a continuum extrapolation based on these lattice spacings and compare them to staggered calculations.

The structure of this letter is the following. In sections 2 and 3 we briefly summarize the overlap and staggered simulation details, respectively. We present the results in section 4 and then conclude. Some important algorithmic details are discussed in the appendix.

## 2. Overlap simulation details

Since we extend our preliminary study [14] we employ the same lattice action, which is described in detail there. For completeness we summarize our setup here:

- tree level Symanzik improved gauge action with coupling parameter  $\beta$
- two flavors of overlap quarks with the overlap operator defined as

$$D = \left(m_0 - \frac{m}{2}\right) [1 + \gamma_5 \text{sgn}(\gamma_5 W(-m_0))] + m,$$

where  $m$  is the mass of the quark,  $W(-m_0)$  is a two step HEX smeared Wilson operator with a negative mass of  $-m_0 = -1.3$ . The HEX smearing parameters are  $\alpha_1 = 0.72$ ,  $\alpha_2 = 0.60$  and  $\alpha_3 = 0.44$ .

- two flavors of Wilson fermions with mass  $-m_0$ , which are irrelevant in the continuum limit [18].
- two boson fields with mass  $m_B = 0.54$  and the action

$$\phi^\dagger [W(-m_0) + im_B \gamma_5 \tau_3] \phi,$$

which term is also irrelevant in the continuum limit.

- ensembles are generated using the Hybrid Monte Carlo (HMC) algorithm with the Zolotarev approximation of the sign function [19, 12]. HEX smearing is included in the HMC as described in [20].

The effect of the irrelevant fields is to disable topological sector changes along the HMC trajectories. Note that the action itself does not constrain the topology, it only differs from the QCD action by irrelevant terms. These irrelevant terms give a delta function like contribution to the action at the topological sector boundaries which the continuous HMC trajectories cannot cross. Our aim is to keep the system in the zero topological charge sector.

The scale is set by the  $w_0$  parameter [21] and our line of constant physics (LCP) is defined by the condition  $m_\pi w_0 = 0.312$ . In Ref. [14] we determined the LCP in the range  $\beta = 3.6 \dots 4.1$ . In this work we needed to determine the line of constant physics (LCP) for larger  $\beta$  values. Using two additional simulations on  $32^4$  and  $32^3 \cdot 48$  lattices at  $\beta = 4.2$  and at 4.3, respectively, we obtained the LCP, which is shown on Figure 1.

For the renormalization of the finite temperature results we performed a series of runs on symmetric lattices  $N_s = N_t$ . These are collected in Table 1. The  $w_0$  values, that are used to convert the results to

physical units, are measured on these lattices. For the conversion we use the value  $w_0 = 0.1755 \text{ fm}$ .<sup>1</sup> To check the quality of our LCP determination we also measured the pion mass on these lattices. The  $m_\pi w_0$  values are also given in Table 1.

The finite temperature lattices are simulated at three temporal extents  $N_t = 8, 10$  and  $12$  and with aspect ratio  $r = N_s/N_t = 2$ . Details can be found in Table 2. The trajectories were generated in two streams. We monitored the topological charge ( $Q$ ) during the simulations: no sector change was observed even though the finite stepsize integration does not necessarily forbid the change. We measured the quark number susceptibility and the chiral condensate on every fifth trajectory.

For the renormalization [2] of the Polyakov loop,  $L$ , we carried out simulations at  $T = 208 \text{ MeV}$  with temporal extents  $N_t = 4, 5, 6, 7, 8, 10, 12$  and  $14$ . We measured the Polyakov loop to obtain the renormalization factor  $F_0(\beta) = 1/N_t \log L$ .

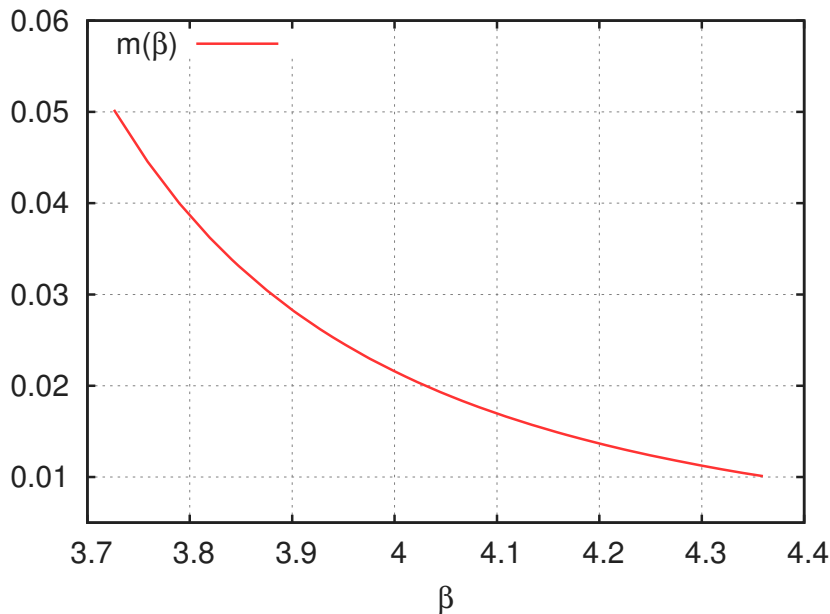


Figure 1: The line of constant physics used in this work.

### 3. Staggered simulation details

In order to compare the continuum results obtained from different discretizations we also performed a series of staggered runs. We used the same tree level Symanzik improved gauge action with  $\beta$  coupling as in the overlap case. The fermion action is a two flavor (rooted) staggered fermion action with four steps of stout smearing with smearing parameter  $\rho = 0.125$ . We tuned the quark mass to the same LCP as in the overlap case ( $m_\pi w_0 = 0.312$ ). To this end we generated 1000-7000 configurations separated by 5 HMC trajectories on  $32^3 \cdot 64$ ,  $40^3 \cdot 64$  and  $48^3 \cdot 64$  lattices in the range  $\beta = 3.75 \dots 4.4$ . These  $T = 0$  runs are also used for renormalization of the chiral observables. At non-vanishing temperature we used  $N_t = 8, 10, 12$  and  $16$  lattices with the same fixed  $r = 2$  aspect ratio as in the overlap case. This guarantees that the same physical volumes are compared. We chose the couplings such that they correspond to the same fixed temperatures at each  $N_t$ . Each ensemble consists of 1000-2000 configurations separated by 10 HMC trajectories. Since in the staggered case the topology was not constrained, all our runs sample multiple topological sectors. In

<sup>1</sup>Note that this choice is ambiguous since this value corresponds to QCD with physical quark masses. Using a different observable to set the scale might lead to somewhat different results in physical units.

$\beta$	$N_s$	#traj	a[fm]	$m_\pi w_0$
3.72601	24	500	0.207	0.310(1)
3.78989	24	600	0.182	0.314(1)
3.84097	24	800	0.165	0.312(2)
3.95191	24	1100	0.135	0.310(2)
4.04464	24	1700	0.115	0.305(2)
4.13912	24	2100	0.096	0.316(5)
4.24969	24	2300	0.079	0.330(8)
4.35979	24	2200	0.066	0.325(17)
4.20588	32	1000	0.087	0.299(5)
4.31965	32	1200	0.070	0.331(9)

Table 1: Summary of zero temperature runs.

$\beta$	$N_t \times N_s$	#traj
3.72601	$8 \times 16$	6300
3.78989	$8 \times 16$	7600
3.84797	$8 \times 16$	9000
3.90165	$8 \times 16$	10500
3.95191	$8 \times 16$	12100
3.99943	$8 \times 16$	13400
4.04464	$8 \times 16$	14400
4.10869	$8 \times 16$	15700
3.84097	$10 \times 20$	6700
3.90810	$10 \times 20$	8200
3.97002	$10 \times 20$	9800
4.02793	$10 \times 20$	11200
4.08253	$10 \times 20$	12300
4.13412	$10 \times 20$	13200
4.18274	$10 \times 20$	13800
4.24969	$10 \times 20$	14100
3.93963	$12 \times 24$	5800
4.01093	$12 \times 24$	6800
4.07720	$12 \times 24$	6100
4.13912	$12 \times 24$	10100
4.19672	$12 \times 24$	11000
4.24969	$12 \times 24$	11400
4.29763	$12 \times 24$	11600
4.35979	$12 \times 24$	10300

Table 2: Summary of finite temperature runs.

the infinite volume limit our observables are expected to be independent of the global topological charge but at the volumes studied in this work there may still be significant  $1/V$  volume corrections [22]. To investigate these effects we also selected gauge configurations with zero topological charge. This makes a direct comparison with the overlap results possible and the difference compared to having all sectors gives an estimate of this volume dependence for each observable. For the selection we applied a gradient flow on the gauge configurations. After measuring the topological charge distribution on these gauge fields we were always able to identify a peak in the histogram which belonged to the  $Q = 0$  sector. We checked that this selection, and, in particular, the resulting expectation value of the chiral condensate, was independent of the  $t$  flow time if  $T^2 t \geq 0.0625$ . For all lattice spacings and temperatures we used the selection rule  $-0.5 < Q(t = 0.0625/T^2) < 0.5$ . Note that by dropping the  $Q \neq 0$  sectors we lost 85% of our statistics below  $T_c$ , in the deconfined phase this loss was only about 10%.

## 4. Results

### 4.1. Continuum extrapolation

We want to compare continuum extrapolated results of temperature dependent observables using two discretizations. This requires a non-trivial analysis, since both an interpolation in  $T$  and a continuum extrapolation is needed. In case of the overlap ensembles for all observables we used two independent analyses following different strategies. These are similar to those applied in [10, 11]. In the first approach we first interpolate the data in temperature for each lattice spacing and then perform a continuum extrapolation at fixed temperatures. The interpolation is done using a cubic spline. The continuum extrapolation is performed as a linear fit in  $1/N_t^2$  using our three lattice spacings. The continuum extrapolations for all observables had good fit qualities.

In the second approach a given observable is interpolated using a functional form of  $O(T) = A(T) + B(T)/N_t^2$  where  $A(T)$  and  $B(T)$  are cubic spline functions. The two splines have the same node points. These, however, do not coincide with the data points. The number of node points is smaller than the number of data points and the  $A(T)$  and  $B(T)$  splines are fitted to the data. The node points are scattered randomly in the temperature range with the following constraints: there is always a node point before the first and after the last data point and in each interval between adjacent data points there can be 0 or 1 node point. In order to determine the systematic uncertainty of the resulting  $O(T)$  curve we weight the various splines using the Akaike Information Criterion (AIC) [23, 24, 25]. The weight of each fit result is  $w_i = \exp(AIC_i/2)$  with  $AIC_i = 2k_i - \chi_i^2$  where  $k_i$  is the number of degrees of freedom and  $\chi_i^2$  is the usual  $\chi^2$  for the  $i^{\text{th}}$  fit. Since there are many possibilities to select node points instead of evenly distributing them we used importance sampling based on the AIC weights. Thus starting from a random set of node points at each step we propose one of the following changes: adding a new node point, removing one, or shifting one without breaking the above constraints. Then the proposed set of new node points is either accepted or rejected using a Metropolis step with probability:  $p = \min\{1, \exp(\Delta AIC/2)\}$ . Since the number of degrees of freedom  $k_i$  (i.e. the number of node points) can change during the Monte-Carlo sampling of node points, bad fit qualities result in small  $k_i$ . In the extreme case when the data is highly inconsistent with the above functional form (i.e. the lattice spacings are far from the scaling regime) the AIC weights are maximized by having no degree of freedom and consequently vanishing  $\chi^2$ . We do not observe such behavior for any of our observables, the required number of degrees of freedom is always  $\mathcal{O}(10)$ , proving that the continuum extrapolations are under control. The resulting  $O(T)$  curves can simply be averaged and the width of their distribution defines our systematic uncertainty. Statistical errors are determined by a jackknife analysis.

The two analyses gave consistent results in all cases. The results presented in the following were obtained with the second one.

As mentioned previously the staggered ensembles were tuned to have the same temperatures for all  $N_t$ . This makes a pointwise continuum extrapolation trivial. The systematic error has been estimated from continuum extrapolations using all four lattice spacings or only the finest three.

#### 4.2. Observables

The first observable we determine is the isospin susceptibility which is the connected part of the quark number susceptibility, defined as:

$$\chi_I = \frac{T}{V} \left. \frac{\partial^2}{\partial \mu_I^2} \right|_{\mu_I=0} \log Z$$

We perform a tree level improvement using the correction factors listed in Table 1 of [14]. Figure 2 shows the results on the three lattice spacings and their continuum extrapolation as well as the staggered continuum result using only the  $Q = 0$  configurations. There is a nice agreement between the two discretizations.

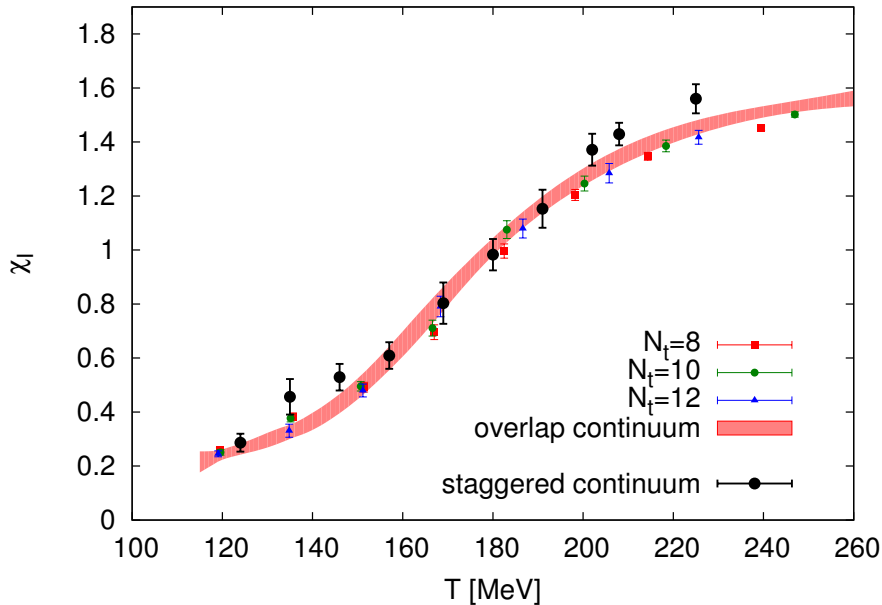


Figure 2: Isospin susceptibility as a function of temperature. The red, green, and blue symbols show the overlap results on  $N_t = 8, 10, 12$  lattices and the purple band is their continuum extrapolation. The continuum extrapolated staggered result using only the  $Q = 0$  configurations is shown by the black dots.

The second observable is the Polyakov loop. The renormalization condition is  $L_R|_{T=208\text{MeV}} = 1$ , according to which we have

$$L_R = L \exp(-N_t F_0(\beta)),$$

where the determination of  $F_0(\beta)$  is described in Section 2. It is shown on Figure 3 again together with the staggered result. In case of the Polyakov loop the selection of  $Q = 0$  configurations at low temperatures causes a significant loss of statistics at  $N_t = 16$  which results in large errors after continuum extrapolation. We checked on the  $N_t = 8$  and  $10$  lattices that this selection has no effect on the result, therefore we show the continuum extrapolated Polyakov loop obtained from all sectors. The continuum extrapolations of the two discretizations are again consistent with each other.

The third observable is the chiral condensate. On Figure 4 we show

$$m_R \bar{\psi} \psi_R w_0^4 = m \left[ \frac{T}{V} \frac{\partial}{\partial m} \log Z \right]_{\text{sub}},$$

where  $[\dots]_{\text{sub}}$  means the zero temperature subtracted value. The staggered result again corresponds to the  $Q = 0$  topological sector.

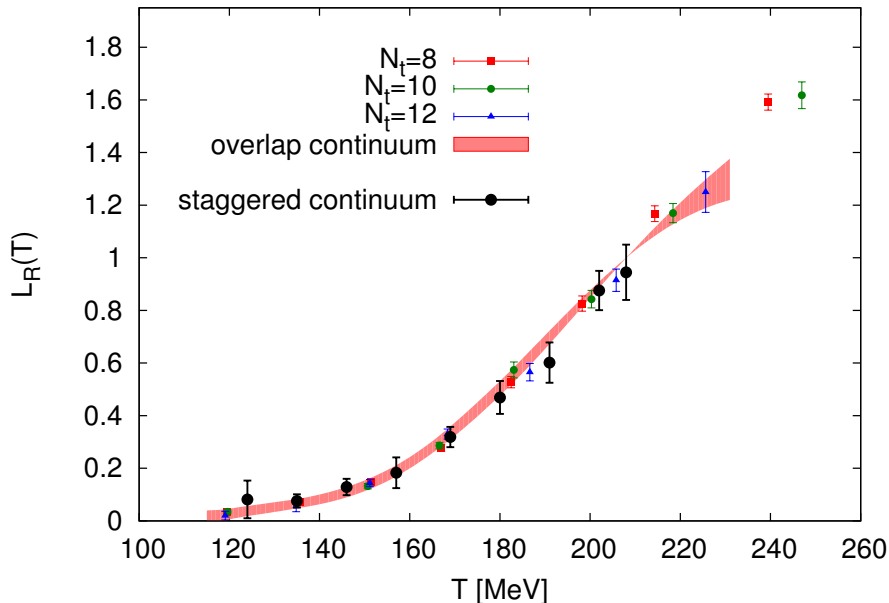


Figure 3: Polyakov loop as a function of temperature. The symbols are the same as in Figure 2. Since no topology dependence is observed the staggered result contains all topological sectors.

The fourth observable is the chiral susceptibility. On Figure 5 we show

$$m_R^2 \chi_{\bar{\psi}\psi_R} w_0^4 = m^2 \left[ \frac{T}{V} \frac{\partial^2}{\partial m^2} \log Z \right]_{\text{sub}}$$

obtained both from the overlap and staggered ensembles. For both chiral observables we see again a nice agreement between overlap and staggered results.

Let us now discuss the effect of fixed topology. Using the full staggered ensembles we can quantify how much our observables depend on the global topology in these relatively small volumes. The quark number susceptibility and Polyakov loop are completely insensitive, using the full ensembles give consistent results but with smaller errors due to using the full statistics. The chiral observables, however show a different behavior, there is a significant difference between using  $Q = 0$  and using all sectors. This is demonstrated in Figure 6 where the continuum extrapolated chiral condensate is shown for these two ensembles. The difference is expected to scale with  $1/V$  therefore using an aspect ratio of  $r = 4$  which is typical for previous staggered studies, it is smaller by an order of magnitude.

## 5. Conclusions

We have presented continuum extrapolated results for the temperature dependence of four observables, the isospin susceptibility, the Polyakov loop, the chiral condensate, and the chiral susceptibility using two flavors of dynamical overlap fermions with a pion mass of  $\approx 350$  MeV. Three temporal extents,  $N_t = 8, 10$  and  $12$  were used which made a controlled continuum extrapolation possible. All runs were performed at fixed topology. The results were compared to continuum extrapolated staggered ones and a nice agreement was found for all observables when the topology was also constrained on the staggered ensembles. Using the full staggered ensembles as well we could estimate the finite volume effect caused by fixing the topology. The isospin susceptibility and the Polyakov loop show no  $Q$  dependence already on these relatively small volumes. The chiral observables, on the other hand, still depend on  $Q$ . It is also possible to perform simulations in different sectors and use the topological susceptibility to combine them [26].

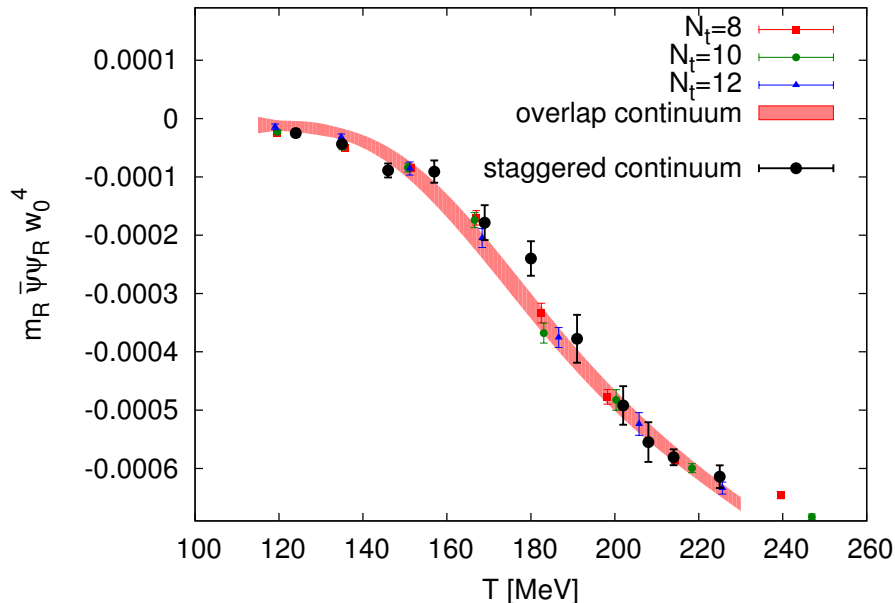


Figure 4: Chiral condensate as a function of temperature. The symbols are the same as in Figure 2. The staggered result corresponds to  $Q = 0$ .

## 6. Acknowledgments

We thank G. Bali, T.W. Chiu, G. Endrodi and A. Schaefer for useful discussions. Computations were performed on JUQUEEN at FZ-Jülich and on GPU clusters at Wuppertal and Budapest. This project was funded by the DFG grant SFB/TR55, by OTKA under grants OTKA-NF-104034 and OTKA-K-113034. S.D.K. is funded by the "Lendület" program of the Hungarian Academy of Sciences (LP2012-44/2012).

## Appendix A. Methods and algorithms

### Appendix A.1. Preconditioning the inverse of the overlap matrix

Beyond the algorithmic ingredients already applied in Ref [14], i.e. Hasenbusch trick [27], Omelyan integrator [28] and a multi-scale scheme [29], a major algorithmic improvement in this work is the preconditioner for the inversion of the overlap matrix. The technique was proposed in [30].

The inverter is the FGMRES algorithm. The preconditioner is the inverse of the Wilson operator with a mass, that is a tuneable parameter. We add a clover term to the Wilson operator, since it makes the preconditioning more efficient: it brings the physical spectrum of the Wilson operator closer to the spectrum of the overlap operator. We utilize an even-odd preconditioned BICGSTAB inverter to invert the Wilson matrix. Since it is still a subdominant part of the total inverter, we did not implement the multigrid acceleration for the Wilson inverse, that was proposed in [30]. The preconditioner utilizes single precision arithmetics.

In the HMC update the inverse of the overlap operator is required at three different occasions: in the heatbath, in the pseudofermion action and in the pseudofermion force. We use two flavors, so in principle the inverse of the square of the overlap operator  $(D^\dagger D)^{-1}$  is needed. The cases of the heatbath and the pseudofermion action simplify to the application of only  $D^{-1}$  for which we can use the preconditioned inverter. In the case of the fermion force we use two consecutive application of the preconditioned inverter:  $(D^\dagger D)^{-1} = D^{-1} \gamma_5 D^{-1} \gamma_5$ . Even this two step approach is about a factor five faster compared to the previously used technique (relaxed CG).

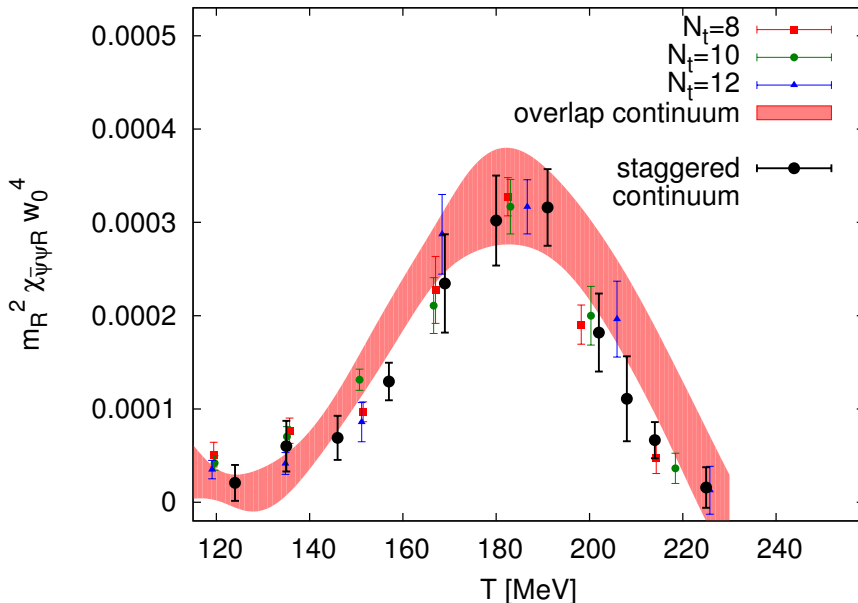


Figure 5: Chiral susceptibility as a function of temperature. The symbols are the same as in Figure 2. The staggered result corresponds to  $Q = 0$ .

#### Appendix A.2. Algorithm to determine the index

Although the action is designed to keep the overlap simulations in fixed sectors, due to the finite stepsize HMC integration sector changes are in principle possible. Therefore it is important to monitor that topology is indeed fixed. Below we discuss how we determined the topological charge using the index of the overlap operator.

The topological charge of a gauge configuration is given by the index  $Q = n_- - n_+$  of the massless overlap operator  $D_0$ , where  $n_-$  and  $n_+$  denote the number of zero modes with negative and positive chirality, respectively. We systematically look for the lowest eigenvalues of  $D_0^\dagger D_0$ , and stop when the first nonzero eigenvalue is found.

The method we apply to find the zero modes, described in Algorithm 1, is based on the inverse iteration. For this one inverts the  $D_0^\dagger D_0$  with a shift  $\sigma$ , which is a fixed parameter of the algorithm. There are three parameters controlling the precision of the eigenmodes, they have to obey the constraint  $0 < \varepsilon_{\text{stop}} \leq \varepsilon_{\text{zero}} \leq \varepsilon_{\text{nonzero}}$ . Parameter  $\varepsilon_{\text{stop}}$  controls the condition when an eigenvector is considered precise enough for the algorithm to stop iterating over it. It is still used for the orthogonalization process. A vector is considered as a zero mode if the corresponding eigenvalue is compatible with zero with an error less than  $\varepsilon_{\text{zero}}$ . A vector is considered as nonzero if the corresponding eigenvalue is different from zero with an error less than  $\varepsilon_{\text{nonzero}}$ .

The inversion in line 14 of Algorithm 1 is computed as two consecutive inversions:

$$\left(D_0^\dagger D_0 + \sigma\right)^{-1} = \left(D_0 + i\gamma_5 \sqrt{\sigma}\right)^{-1} \gamma_5 \left(D_0 - i\gamma_5 \sqrt{\sigma}\right)^{-1} \gamma_5. \quad (\text{A.1})$$

The inversions of  $D_0 \pm i\gamma_5 \sqrt{\sigma}$  are performed using the FGMRES inverter, as described in Subsection Appendix A.1. For the shift  $\sigma$  we chose a positive value, tuned such that it allows for a rapid convergence in the inversions, while keeps the number of iterations in Algorithm 1 as low as possible. In addition, a positive value of  $\sigma$  ensures that the zero eigenmodes are found first.

As an example, using the parameter values  $\varepsilon_{\text{stop}} = 10^{-8}$ ,  $\varepsilon_{\text{zero}} = 10^{-6}$ ,  $\varepsilon_{\text{nonzero}} = 10^{-4}$  and  $\sigma = 10^{-4}$  on a  $12 \times 24^3$  lattice with  $Q = -3$ , the algorithm found the three zero modes and the first nonzero mode within 8 iterations.

---

**Algorithm 1** Inverse iteration to find index of overlap operator
 

---

```

1: procedure INDEX( $\sigma, \varepsilon_{\text{nonzero}}, \varepsilon_{\text{zero}}, \varepsilon_{\text{stop}}$ )
2:    $i \leftarrow 0$  ▷ The index will be stored in  $i$ .
3:    $n_{\text{zero}} \leftarrow 0, n_{\text{vec}} \leftarrow 0$  ▷ Start without vectors.
4:   repeat
5:     if  $n_{\text{zero}} = n_{\text{vec}}$  then ▷ If all vectors are zero modes,
6:        $n_{\text{vec}} \leftarrow n_{\text{vec}} + 1$  ▷ introduce a new vector.
7:        $v_{n_{\text{vec}}} \leftarrow$  Gaussian random vector
8:       
$$v_{n_{\text{vec}}} \leftarrow v_{n_{\text{vec}}} - \sum_{l=1}^{n_{\text{vec}}-1} \langle v_l | v_{n_{\text{vec}}} \rangle v_l$$

9:       
$$v_{n_{\text{vec}}} \leftarrow \frac{v_{n_{\text{vec}}}}{\|v_{n_{\text{vec}}}\|}$$
 ▷ Orthogonalize w.r.t. previous vectors.
10:       $\varepsilon_{n_{\text{vec}}} \leftarrow \varepsilon_{\text{nonzero}} + 1$ 
11:    end if
12:    for  $k \leftarrow 1$  to  $n_{\text{vec}}$  do
13:      if  $\varepsilon_k > \varepsilon_{\text{stop}}$  then ▷ Don't update if vector is too precise.
14:         $w \leftarrow (D_0^\dagger D_0 + \sigma)^{-1} v_k$  ▷ Invert using FGMRES.
15:         $\mu \leftarrow \langle w | v_k \rangle$ 
16:         $\lambda_k \leftarrow -\sigma + \frac{1}{\mu}$  ▷ Estimate eigenvalue.
17:         $\varepsilon_k \leftarrow \left\| v_k - \frac{w}{\mu} \right\| / \|w\|$  ▷ Estimate error of eigenvalue.
18:        
$$w \leftarrow w - \sum_{l=1}^{k-1} \langle v_l | w \rangle v_l$$

19:        
$$v_k \leftarrow \frac{w}{\|w\|}$$
 ▷ Keep orthonormality of vector set.
20:      end if
21:    end for
22:    if  $(\varepsilon_{n_{\text{vec}}} \leq \varepsilon_{\text{zero}}) \wedge (\lambda_{n_{\text{vec}}} < \varepsilon_{n_{\text{vec}}})$  then
23:       $n_{\text{zero}} \leftarrow n_{\text{zero}} + 1$  ▷ If a zero mode is encountered,
24:       $i \leftarrow i - \text{sgn}[\langle v_{n_{\text{zero}}} | \gamma_5 | v_{n_{\text{zero}}} \rangle]$  ▷ update the index.
25:    end if
26:  until  $(\varepsilon_{n_{\text{vec}}} \leq \varepsilon_{\text{nonzero}}) \wedge (\lambda_{n_{\text{vec}}} > \varepsilon_{n_{\text{vec}}})$  ▷ Found a nonzero eigenvalue.
27:  return  $i$ 
28: end procedure

```

---

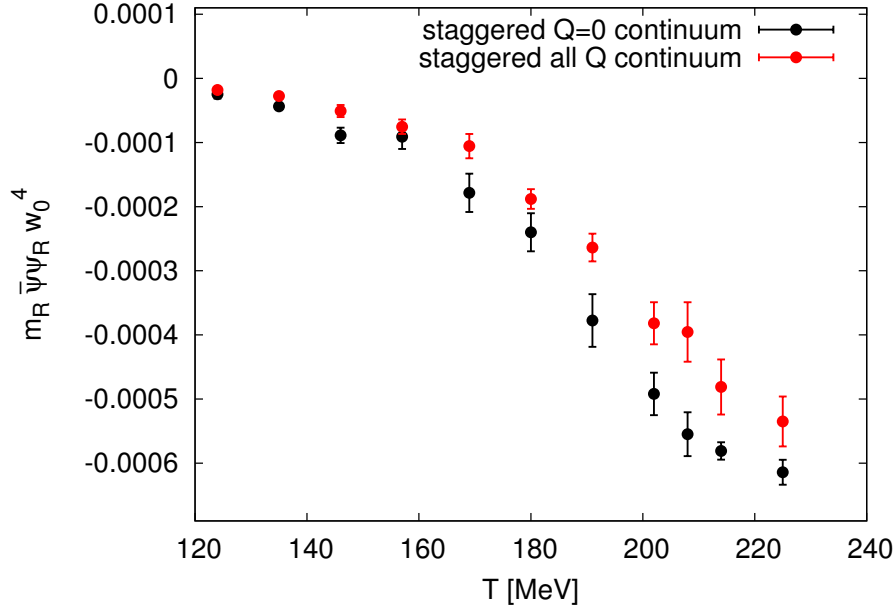


Figure 6: Comparison of the staggered continuum extrapolated chiral condensate in the  $Q = 0$  sector and in all sectors.

## References

## References

- [1] Y. Aoki, G. Endrodi, Z. Fodor, S. D. Katz, K. K. Szabo, The Order of the quantum chromodynamics transition predicted by the standard model of particle physics, *Nature* 443 (2006) 675–678. [arXiv:hep-lat/0611014](#), [doi:10.1038/nature05120](#).
- [2] Y. Aoki, Z. Fodor, S. D. Katz, K. K. Szabo, The QCD transition temperature: Results with physical masses in the continuum limit, *Phys. Lett. B* 643 (2006) 46–54. [arXiv:hep-lat/0609068](#), [doi:10.1016/j.physletb.2006.10.021](#).
- [3] Y. Aoki, S. Borsanyi, S. Durr, Z. Fodor, S. D. Katz, S. Krieg, K. K. Szabo, The QCD transition temperature: results with physical masses in the continuum limit II., *JHEP* 06 (2009) 088. [arXiv:0903.4155](#), [doi:10.1088/1126-6708/2009/06/088](#).
- [4] S. Borsanyi, Z. Fodor, C. Hoelbling, S. D. Katz, S. Krieg, C. Ratti, K. K. Szabo, Is there still any  $T_c$  mystery in lattice QCD? Results with physical masses in the continuum limit III, *JHEP* 09 (2010) 073. [arXiv:1005.3508](#), [doi:10.1007/JHEP09\(2010\)073](#).
- [5] A. Bazavov, et al., The chiral and deconfinement aspects of the QCD transition, *Phys. Rev. D* 85 (2012) 054503. [arXiv:1111.1710](#), [doi:10.1103/PhysRevD.85.054503](#).
- [6] S. Borsanyi, G. Endrodi, Z. Fodor, A. Jakovac, S. D. Katz, S. Krieg, C. Ratti, K. K. Szabo, The QCD equation of state with dynamical quarks, *JHEP* 11 (2010) 077. [arXiv:1007.2580](#), [doi:10.1007/JHEP11\(2010\)077](#).
- [7] S. Borsanyi, Z. Fodor, C. Hoelbling, S. D. Katz, S. Krieg, K. K. Szabo, Full result for the QCD equation of state with 2+1 flavors, *Phys. Lett. B* 730 (2014) 99–104. [arXiv:1309.5258](#), [doi:10.1016/j.physletb.2014.01.007](#).
- [8] A. Bazavov, et al., Equation of state in (2+1)-flavor QCD, *Phys. Rev. D* 90 (9) (2014) 094503. [arXiv:1407.6387](#), [doi:10.1103/PhysRevD.90.094503](#).
- [9] R. Bellwied, S. Borsanyi, Z. Fodor, S. D. Katz, A. Pasztor, C. Ratti, K. K. Szabo, Fluctuations and correlations in high temperature QCD, [arXiv:1507.04627](#).
- [10] S. Borsanyi, S. Durr, Z. Fodor, C. Hoelbling, S. D. Katz, S. Krieg, D. Negradi, K. K. Szabo, B. C. Toth, N. Trombitas, QCD thermodynamics with continuum extrapolated Wilson fermions I, *JHEP* 08 (2012) 126. [arXiv:1205.0440](#), [doi:10.1007/JHEP08\(2012\)126](#).
- [11] S. Borsanyi, S. Durr, Z. Fodor, C. Hoelbling, S. D. Katz, S. Krieg, D. Negradi, K. K. Szabo, B. C. Toth, N. Trombitas, QCD thermodynamics with continuum extrapolated Wilson fermions II, *Phys. Rev. D* 92 (1) (2015) 014505. [arXiv:1504.03676](#), [doi:10.1103/PhysRevD.92.014505](#).
- [12] Z. Fodor, S. D. Katz, K. K. Szabo, Dynamical overlap fermions, results with hybrid Monte Carlo algorithm, *JHEP* 08 (2004) 003. [arXiv:hep-lat/0311010](#), [doi:10.1088/1126-6708/2004/08/003](#).
- [13] G. Cossu, S. Aoki, H. Fukaya, S. Hashimoto, T. Kaneko, H. Matsufuru, J.-I. Noaki, Finite temperature study of the axial  $U(1)$  symmetry on the lattice with overlap fermion formulation, *Phys. Rev. D* 87 (11) (2013) 114514, [Erratum: *Phys. Rev. D* 88, no.1, 019901(2013)]. [arXiv:1304.6145](#), [doi:10.1103/PhysRevD.87.114514](#), [doi:10.1103/PhysRevD.88.019901](#).

- [14] S. Borsanyi, Y. Delgado, S. Durr, Z. Fodor, S. D. Katz, S. Krieg, T. Lippert, D. Nogradi, K. K. Szabo, QCD thermodynamics with dynamical overlap fermions, *Phys. Lett. B* 713 (2012) 342–346. [arXiv:1204.4089](#), [doi:10.1016/j.physletb.2012.06.022](#).
- [15] M. I. Buchoff, et al., QCD chiral transition,  $U(1)_A$  symmetry and the dirac spectrum using domain wall fermions, *Phys. Rev. D* 89 (5) (2014) 054514. [arXiv:1309.4149](#), [doi:10.1103/PhysRevD.89.054514](#).
- [16] T.-W. Chiu, W.-P. Chen, Y.-C. Chen, H.-Y. Chou, T.-H. Hsieh, Chiral symmetry and axial  $U(1)$  symmetry in finite temperature QCD with domain-wall fermion, *PoS LATTICE2013* (2014) 165. [arXiv:1311.6220](#).
- [17] T. Bhattacharya, et al., QCD Phase Transition with Chiral Quarks and Physical Quark Masses, *Phys. Rev. Lett.* 113 (8) (2014) 082001. [arXiv:1402.5175](#), [doi:10.1103/PhysRevLett.113.082001](#).
- [18] H. Fukaya, S. Hashimoto, K.-I. Ishikawa, T. Kaneko, H. Matsufuru, T. Onogi, N. Yamada, Lattice gauge action suppressing near-zero modes of  $H(W)$ , *Phys. Rev. D* 74 (2006) 094505. [arXiv:hep-lat/0607020](#), [doi:10.1103/PhysRevD.74.094505](#).
- [19] J. van den Eshof, A. Frommer, T. Lippert, K. Schilling, H. A. van der Vorst, Numerical methods for the QCD overlap operator. I. Sign function and error bounds, *Comput. Phys. Commun.* 146 (2002) 203–224. [arXiv:hep-lat/0202025](#), [doi:10.1016/S0010-4655\(02\)00455-1](#).
- [20] S. Durr, Z. Fodor, C. Hoelbling, S. D. Katz, S. Krieg, T. Kurth, L. Lellouch, T. Lippert, K. K. Szabo, G. Vulvert, Lattice QCD at the physical point: Simulation and analysis details, *JHEP* 08 (2011) 148. [arXiv:1011.2711](#), [doi:10.1007/JHEP08\(2011\)148](#).
- [21] S. Borsanyi, et al., High-precision scale setting in lattice QCD, *JHEP* 09 (2012) 010. [arXiv:1203.4469](#), [doi:10.1007/JHEP09\(2012\)010](#).
- [22] S. Aoki, H. Fukaya, S. Hashimoto, T. Onogi, Finite volume QCD at fixed topological charge, *Phys. Rev. D* 76 (2007) 054508. [arXiv:0707.0396](#), [doi:10.1103/PhysRevD.76.054508](#).
- [23] H. Akaike, Information theory and an extension of the maximum likelihood principle, in: B. Petrov, F. Csaki (Eds.), 2nd International Symposium on Information Theory, Akademiai Kiado, Budapest, 1973, pp. 267–281.
- [24] H. Akaike, On the likelihood of a time series model, *The Statistician* 27 (1978) 217–235.
- [25] S. Borsanyi, et al., Ab initio calculation of the neutron-proton mass difference, *Science* 347 (2015) 1452–1455. [arXiv:1406.4088](#), [doi:10.1126/science.1257050](#).
- [26] G. I. Egri, Z. Fodor, S. D. Katz, K. K. Szabo, Topology with dynamical overlap fermions, *JHEP* 01 (2006) 049. [arXiv:hep-lat/0510117](#), [doi:10.1088/1126-6708/2006/01/049](#).
- [27] M. Hasenbusch, Speeding up the hybrid Monte Carlo algorithm for dynamical fermions, *Phys. Lett. B* 519 (2001) 177–182. [arXiv:hep-lat/0107019](#), [doi:10.1016/S0370-2693\(01\)01102-9](#).
- [28] T. Takaishi, P. de Forcrand, Testing and tuning new symplectic integrators for hybrid Monte Carlo algorithm in lattice QCD, *Phys. Rev. E* 73 (2006) 036706. [arXiv:hep-lat/0505020](#), [doi:10.1103/PhysRevE.73.036706](#).
- [29] J. C. Sexton, D. H. Weingarten, Hamiltonian evolution for the hybrid Monte Carlo algorithm, *Nucl. Phys. B* 380 (1992) 665–678. [doi:10.1016/0550-3213\(92\)90263-B](#).
- [30] J. Brannick, A. Frommer, K. Kahl, B. Leder, M. Rottmann, A. Strebel, Multigrid Preconditioning for the Overlap Operator in Lattice QCD, *Numer. Math.* [arXiv:1410.7170](#), [doi:10.1007/s00211-015-0725-6](#).